Analytical solution for restricted diffusion in circular and spherical layers under inhomogeneous magnetic fields

Denis S. Grebenkov[a)]
Laboratoire de Physique de la Matière Condensée, CNRS-Ecole Polytechnique, F-91128 Palaiseau, France

(Received 14 November 2007; accepted 11 January 2008; published online 1 April 2008)

We propose an analytical solution for restricted diffusion of spin-bearing particles in circular and spherical layers in inhomogeneous magnetic fields. More precisely, we derive exact and explicit formulas for the matrix representing an applied magnetic field in the Laplacian eigenbasis and governing the magnetization evolution. For thin layers, a significant difference between two geometrical length scales (thickness and overall size) allows for accurate perturbative calculations. In these two-scale geometries, apparent diffusion coefficient (ADC) as a function of diffusion time exhibits a new region with a reduced but constant value. The emergence of this intermediate diffusion regime, which is analogous to the tortuosity regime in porous media, is explained in terms of the underlying Laplace operator eigenvalues. In general, regions with constant ADCs would be reminiscent of multiscale geometries, and their observation can potentially be used in experiments to detect the length scales by varying diffusion time. © *2008 American Institute of Physics*. [DOI: 10.1063/1.2841367]

I. INTRODUCTION

Since the discovery of spin echoes by Hahn in 1950, restricted diffusion of spin-bearing particles in geometrical confinements has often been investigated by applying inhomogeneous magnetic fields (see review[1] and references therein). Since the magnetic field determines the local precession frequency of spins, its spatial inhomogeneities allow to distinguish spatial points in the confining domain, encoding thus the whole trajectory of each spin-bearing particle. The accumulated phase shifts of individual particles result in a collective macroscopic signal, called an echo. The echo amplitude implicitly characterizes restricted diffusion in general and the underlying geometrical confinement, in particular. For instance, in the slow-diffusion or short-time regime, Mitra *et al.*[2,3] showed that the macroscopic signal depends on the surface-to-volume ratio of a statistically isotropic sample (see also Sen[4]). In the opposite long-time diffusion limit, predicted by Robertson[5] and experimentally observed by Wayne and Cotts[6] in a slab, the macroscopic signal is very sensitive to the slab width. Later, Neuman extended this result to the case of a cylinder and a sphere.[7] Callaghan *et al.* employed (short-) pulsed-gradient spin-echo techniques to study diffusion diffraction for characterization of porous media.[8–10]

Among various theoretical approaches, the spectral theory involving Laplace operator eigenbasis was recognized to be particularly efficient to describe diffusive motion in a geometrical confinement. For instance, Brownstein and Tarr employed this description in order to explain multiexponential relaxation for water in biological cells.[11] More general matrix formalisms have been developed during the past decade for both numerical and theoretical studies of restricted diffusion in NMR.[1,12–17] We briefly discuss these formalisms in Sec. II.

Even in the case of a slab, the simplest confining geometry, there is no simple explicit formula describing the attenuation of the macroscopic signal in a linear magnetic-field gradient. The emergence of the aforementioned diffusion regimes is conditioned by three ratios p, q, and h between four characteristic length scales: geometrical length L (confinement size); diffusion length $\sqrt{DT}$, showing the average distance explored by spins with the free diffusion coefficient D during time T; gradient length $(\gamma g T)^{-1}$, over which the magnetic-field gradient g yields a phase spread of the order of 2π (γ being the gyromagnetic ratio of spins); and relaxation length D/ρ, which is the distance a spin-bearing particle should travel near the boundary before surface relaxivity ρ reduces its expected magnetization:

$$p = DT/L^2, \quad q = \gamma g T L, \quad h = \rho L/D. \tag{1}$$

Most theoretical and numerical studies have been realized for three simple geometrical confinements: a slab, a cylinder, and a sphere. Actually, when the applied gradient is orthogonal to the slab plates or to the cylinder axis, displacements along these plates or along this axis are irrelevant, and the problem becomes, respectively, one and two dimensional (restricted diffusion on an interval and in a disk). In all three cases, the Laplace operator eigenfunctions are known, allowing to derive a number of analytical results. For instance, Neuman used these eigenfunctions to obtain accurate approximate formulas for the macroscopic signal attenuation due to the restricted diffusion in these three domains.[7] His results have recently been extended to include surface relaxivity.[18] Many other facts about restricted diffusion in these domains are reported in our review.[1]

In spite of recent progresses in this field, there still exists a substantial "gap" in understanding restricted diffusion in

[a)]Electronic mail: denis.grebenkov@polytechnique.edu.

simple geometrical confinements on the one hand, and in natural porous media such as sedimentary rocks, cements, or biological tissues, on the other hand. From theoretical point of view, the complexity of porous structures is related to *multiple length scales*, ranging from the size of tiny pores (in the order of several microns in some rocks) to the overall size of the sample (e.g., few centimeters). Moreover, some porous media present a hierarchical structure of pores so that intermediate characteristic length scales emerge. In this case, even the introduction of representative dimensionless parameters such as p, q, and h becomes ambiguous as being depended on geometrical length L used. It is thus important to understand how classical theories for single-scale shapes (like a slab) should be extended to incorporate multiple scales. Since an analytical calculation in natural porous media is unfeasible, some simplified confinements with two or multiple length scales become particularly useful.

In this paper, we consider the problem of restricted diffusion in two families of rotation-invariant domains, circular and spherical layers, presenting two geometrical lengths (thickness and overall size). Like for a disk and a sphere, the radial and angular coordinates can be separated for these domains, and the Laplace operator eigenfunctions are known. Using the properties of the underlying Bessel equation, we derive explicit analytical formulas for the matrix $\mathcal{B}$ representing a linear magnetic-field gradient (or parabolic magnetic field as well) in the Laplace operator eigenbasis (Sec. III). From the numerical point of view, the problem is completely reduced to finding roots of the equations with Bessel functions. Once these roots are determined, the governing matrices $\mathcal{B}$ and Λ (defined below) can easily be constructed and used to compute the macroscopic signal for any temporal dependence (or profile) of the magnetic field.

Bearing in mind multiscale structures, we particularly focus on thin layers in Sec. IV. In this case, the thickness of the layer is much smaller than its overall size, and surprisingly accurate perturbative calculations are possible. We show that the analysis is, in fact, much simpler for thin layers than for the classical cases of the unit disk or sphere. We derive an explicit formula for the apparent diffusion coefficient and discuss the emergence of a new intermediate regime analogous to the tortuosity regime in porous media. The transition from the slow diffusion to this intermediate regime and then to the motional-narrowing regime is investigated in detail. The role of the underlying Laplace operator eigenvalues is discussed. A similar mechanism is conjectured to be at the origin of the tortuosity regime in statistically isotropic porous media. Several significant though technical issues are reported in Appendixes.

II. MULTIPLE CORRELATION FUNCTION DESCRIPTION

In this section, we recall the main concepts, notations, and relations of the multiple correlation function (MCF) description following Ref. 1. The evolution of magnetization $\mathfrak{m}(\mathbf{r},t)$ in an applied magnetic field $B(\mathbf{r},t)$ is described by Bloch–Torrey equation,

$$\left(\frac{\partial}{\partial t} - D\Delta + i\gamma B(\mathbf{r},t)\right)\mathfrak{m}(\mathbf{r},t) = 0,$$

where $\Delta = \partial^2/\partial_1^2 + \cdots + \partial^2/\partial_d^2$ is the Laplace operator in d dimensions, and i is the imaginary unit. In most cases of practical interest, the spatial and temporal variations of the magnetic field are factored. Note that the spatial variation $B(\mathbf{r})$ is often a linear gradient of intensity g in a fixed direction, while the effective temporal profile $f(t)$ takes into account the refocusing 180° rf pulse (this scheme can also be applied to stimulated echoes[1,19]).

For theoretical analysis, it is convenient to write this equation in dimensionless units introduced in Eq. (1),

$$\left(\frac{\partial}{\partial t} - pL^2\Delta + iqf(t)B(\mathbf{r})\right)\mathfrak{m}(\mathbf{r},t) = 0.$$

Here, t is the dimensionless time varying from 0 (the first 90° rf pulse) to 1 (the formation of a spin echo). When the 90° rf pulse is spatially homogeneous, the initial magnetization is simply proportional to the initial density $\rho(\mathbf{r})$ of spins: $\mathfrak{m}(\mathbf{r},t=0) = \rho(\mathbf{r})$. Robin boundary condition is imposed to account for the effects of surface relaxation

$$L\frac{\partial}{\partial n}\mathfrak{m}(\mathbf{r},t) + h\mathfrak{m}(\mathbf{r},t) = 0,$$

where $\partial/\partial n$ is the normal derivative on the boundary $\partial\Omega$ directed outward the bulk. When there is no surface relaxation ($h=0$), this relation is reduced to Neumann boundary condition.

Solving this boundary value problem in a given confining domain Ω, one obtains the magnetization at time $t=1$ and integrates it over the whole sample with a given pickup function $\tilde{\rho}(\mathbf{r})$ of the coil or antenna

$$E = \int_\Omega d\mathbf{r}\, \mathfrak{m}(\mathbf{r},1)\, \tilde{\rho}(\mathbf{r}).$$

For a constant temporal profile $f(t)=1$, the macroscopic signal can be obtained by a perturbation theory in a compact matrix form:[1,14–16,20]

$$E = (Ue^{-(p\Lambda + iq\mathcal{B})}\tilde{U}), \tag{2}$$

where the infinite-dimensional matrices $\mathcal{B}$ and Λ and vectors U and $\tilde{U}$ are defined as

$$\Lambda_{m,m'} = \delta_{m,m'}\lambda_m, \tag{3}$$

$$\mathcal{B}_{m,m'} = \int_\Omega d\mathbf{r}\, u_m^*(\mathbf{r})\, B(\mathbf{r})\, u_{m'}(\mathbf{r}), \tag{4}$$

$$U_m = V^{1/2}\int_\Omega d\mathbf{r}\, u_m^*(\mathbf{r})\, \rho(\mathbf{r}), \tag{5}$$

$$\tilde{U}_m = V^{-1/2}\int_\Omega d\mathbf{r}\, u_m(\mathbf{r})\, \tilde{\rho}(\mathbf{r}), \tag{6}$$

asterisk denoting the complex conjugate, V being the volume of the domain, $\delta_{m,m'}$ the Kronecker symbol, $u_m(\mathbf{r})$ the

Laplace operator eigenfunctions, and λ_m the associated (dimensionless) eigenvalues:

$$L^2\Delta u_m(\mathbf{r}) + \lambda_m u_m(\mathbf{r}) = 0 \quad \text{in } \Omega, \tag{7}$$

$$L\frac{\partial}{\partial n}u_m(\mathbf{r}) + h u_m(\mathbf{r}) = 0 \quad \text{on } \partial\Omega. \tag{8}$$

The eigenfunctions $u_m(\mathbf{r})$ are orthogonal, and we use the normalization condition

$$\int_\Omega d\mathbf{r}\, u_m^*(\mathbf{r})\, u_{m'}(\mathbf{r}) = \delta_{m,m'}. \tag{9}$$

The matrix representation (2) easily extends to any piecewise-constant temporal profile $f(t)$ taking the value f_k on the time interval $t \in (t_k, t_{k+1})$ $(k=0,\ldots,K-1)$, with $t_0=0$ and $t_K=1$:

$$E = \left(U \left[\prod_{k=0}^{K-1} e^{-(p\Lambda + iqf_k\mathcal{B})(t_{k+1}-t_k)} \right] \tilde{U} \right). \tag{10}$$

This result is exact; no simplifying approximation was used. Since a given temporal profile $f(t)$ can always be approximated by a piecewise-constant function, the above relation serves as a mathematical foundation for an approximate numerical computation of the macroscopic signal for arbitrary $f(t)$. The efficiency of this numerical technique is based upon an unbounded increase of the eigenvalues λ_m with m: the matrix Λ standing in the argument of the exponential function allows one to truncate the infinite-dimensional matrices $\mathcal{B}$ and Λ to moderate sizes.

The above macroscopic description is very efficient for numerical computations. However, a theoretical analysis is still a difficult task because the matrices $\mathcal{B}$ and Λ do not commute. An alternative microscopic description is often employed in this case (see review[1] and references therein). In this frame, the macroscopic signal is related to an ensemble average of the total dephasing ϕ accumulated by individual spins during their motion in a time-dependent spatially inhomogeneous magnetic field

$$\phi = \int_0^1 dt\, f(t)\, B(X_t),$$

ϕ being here a random variable depending on the stochastic trajectory X_t of a spin-bearing particle. Since the number of these particles is usually extremely large, the ensemble average can be replaced by expectation over all Brownian paths:

$$E = \mathbb{E}\{e^{iq\phi}\}.$$

If the random phase ϕ had a Gaussian distribution, the macroscopic signal would be fully determined by the second moment. Although it is rigorously true only for a free (unrestricted) diffusion, this "Gaussian-phase approximation" is reasonably applicable in many cases of practical interest:

$$E \approx \exp[-q^2\mathbb{E}\{\phi^2/2\}]. \tag{11}$$

For weak gradients (small q), the second moment is the major contribution, while higher-order moments may provide corrections. All the moments can be expressed through the matrices $\mathcal{B}$ and Λ and vectors U and $\tilde{U}$ as

$$\mathbb{E}\{\phi^n/n!\} = \int_0^1 dt_1 f(t_1) \ldots \int_{t_{n-1}}^1 dt_n f(t_n) \times (U e^{-p\Lambda t_1}\mathcal{B} e^{-p\Lambda(t_2-t_1)}\mathcal{B}\cdots\mathcal{B}e^{-p\Lambda(1-t_n)}\tilde{U}). \tag{12}$$

This formula, or its particular cases, was employed by several authors for theoretical study of restricted diffusion in NMR.

In summary, the matrices $\mathcal{B}$ and Λ, constructed on the basis of the Laplace operator eigenfunctions and eigenvalues, completely determine restricted diffusion and the consequent macroscopic signal attenuation. The above matrix formalism is a general and well-adapted mathematical language to tackle a wide range of related questions, at both theoretical and numerical levels. In what follows, we use this language to describe restricted diffusion and related spin-echo experiments in two particular confinements: circular and spherical layers. For these rotation-invariant domains, the Laplace operator eigenfunctions are well known.[21,22] In particular, the computation of the associated eigenvalues, forming the matrix Λ, is classical. What is new here is the use of these eigenfunctions in the context of the above matrix formalism and further applications in NMR. One of the major contributions of this paper is a rigorous derivation of the exact analytical formulas for the matrix $\mathcal{B}$, governing the evolution of the spin magnetization in a linear magnetic-field gradient (as well as in parabolic magnetic field). As illustrated below, this is an indispensable element for both computational techniques and theoretical analysis.

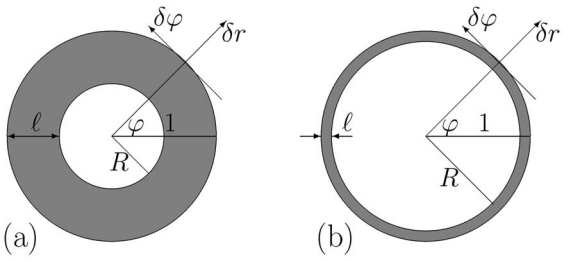

FIG. 1. Circular layers of thickness $\ell = 1-R$ with inner radius R and outer radius $L=1$: $R=0.5$ (a) and $R=0.9$ (b). Note that variations in radial and angular coordinates are orthogonal to each other.

III. ROTATION-INVARIANT DOMAINS

A. Circular layer

We first consider a circular layer $\Omega = \{\mathbf{r} \in \mathbb{R}^2 : R < |\mathbf{r}| < 1\}$ with the inner radius $0 < R < 1$ and the outer radius $L=1$, its boundary $\partial\Omega$ consisting in two circles (Fig. 1). The invariance of this domain under rotations yields separation of the radial and angular variables in Eq. (7). The angular part is simply a Fourier harmonic $e^{in\varphi}$, while the radial part $v(r)$ satisfies the Bessel equation[21,22]

$$r^2v'' + rv' + (\alpha^2 r^2 - n^2)v = 0, \tag{13}$$

where prime denotes the derivative with respect to r, and α^2 is used for the eigenvalue λ. A general solution of this equation is a linear combination of the Bessel functions of the first and second kind:

$$v(r) = c^{(1)}J_n(\alpha r) + c^{(2)}Y_n(\alpha r).$$

Three parameters α, $c^{(1)}$, and $c^{(2)}$ are determined by the chosen normalization (9) and the Robin boundary condition (8) at the inner and outer circles

$$v'(R) - hv(R) = 0, \quad v'(1) + hv(1) = 0 \tag{14}$$

(the signs are different due to the opposite directions of the normal derivative). Note that the dimensionless surface relaxivity h could take different values at the inner and outer boundaries. These boundary conditions imply a closed equation for the parameter α:

$$[\alpha J_n'(\alpha R) - hJ_n(\alpha R)][\alpha Y_n'(\alpha) + hY_n(\alpha)] - [\alpha J_n'(\alpha) + hJ_n(\alpha)][\alpha Y_n'(\alpha R) - hY_n(\alpha R)] = 0. \tag{15}$$

For each n and $0<R<1$, this equation has an infinite set of positive solutions α_{nk} that we distinguish by a pair of indices n and k. Although these solutions have to be computed numerically, the radial part $v(r)$ has explicit functional form. Using the properties of the Bessel equation (13), one can derive a number of analytical results, as illustrated below. As a matter of fact, the computation of α_{nk} is the only nontrivial step of a MCF-based numerical technique.

Bringing together these basic facts, the eigenfunctions are conveniently written as

$$u_{nk}(r,\varphi) = \frac{\epsilon_n}{\sqrt{\pi}}\beta_{nk}\frac{v_{nk}(r)}{v_{nk}(1)}\cos n\varphi, \tag{16}$$

where $\epsilon_n = \sqrt{2}$ for $n>0$, and $\epsilon_0 = 1$, and β_{nk} are the normalization coefficients:

$$\beta_{nk} = \left(\frac{\lambda_{nk}}{[(\lambda_{nk}+h^2)-n^2] - [(\lambda_{nk}+h^2)R^2 - n^2]\xi_{nk}^2}\right)^{1/2}, \tag{17}$$

with

$$\xi_{nk} = \frac{v_{nk}(R)}{v_{nk}(1)}$$

(see Appendix A for details). Note that the enumeration of the eigenvalues and eigenfunctions requires now the double index nk instead of a single index m. In order to return to the single index, the eigenvalues λ_{nk} can be sorted in ascending order (this is also required to truncate the infinite-dimensional matrices $\mathcal{B}$ and Λ for numerical computation). The position of the eigenmode in such a sequence can be assigned as its single index m. In what follows, we shall mostly use the double index as a *convenient notation*. For instance, $\Lambda_{nk,n'k'}$ is not a tensor of rank 4, but still a matrix whose raws and columns are indexed by pairs nk and $n'k'$.

Since the solutions α_{nk} of Eq. (15) determine the eigenvalues, $\lambda_{nk} = \alpha_{nk}^2$, the matrix Λ is readily constructed according to Eq. (3). In turn, the computation of the matrix $\mathcal{B}$, depending on the eigenfunctions and the spatial profile $B(\mathbf{r})$ of the magnetic field, requires substantial work. When a linear magnetic-field gradient applied along the x axis, one needs to calculate the integral

$$\mathcal{B}_{nk,n'k'} = \int_R^1 dr\, r \int_0^{2\pi} d\varphi\, u_{nk}^*(r,\varphi)\, u_{n'k'}(r,\varphi)\, r\cos\varphi.$$

The integration over φ is elementary, yielding

$$\mathcal{B}_{nk,n'k'} = \delta_{n,n'\pm 1}(1 + \delta_{n,0} + \delta_{n',0})^{1/2} \times \frac{\beta_{nk}\beta_{n'k'}}{v_{nk}(1)v_{n'k'}(1)}\int_R^1 dr r^2 v_{nk}(r)v_{n'k'}(r). \tag{18}$$

Given that each function $v_{nk}(r)$ is the combination of two Bessel functions with three parameters α_{nk}, $c_{nk}^{(1)}$, and $c_{nk}^{(2)}$ which are determined implicitly through Eqs. (9) and (14), an analytical computation of the above integral looks as a challenging task. One could instead perform a numerical integration in Eq. (18) for each element of the (truncated) matrix $\mathcal{B}$. However, an accurate integration for the oscillating functions $v_{nk}(r)$ and $v_{n'k'}(r)$ would be the most time-consuming step of a MCF-based numerical technique. Moreover, any further *analytical* investigation involving the elements of the matrix $\mathcal{B}$ would be prohibited (for instance, extension of Neuman's results to circular layers). For this reason, the important, though technical, result of this paper is an exact explicit computation of the above integral under the condition $|n-n'|=1$ which is guaranteed by Kronecker symbol in Eq. (18). This condition, which came from the integration by the angular coordinate, independently from the radial part, is necessary to get a closed explicit formula. For instance, if the magnetic field was $r\cos 2\varphi$ instead of $r\cos\varphi$, this computation would probably be unfeasible. We perform this derivation in Appendix A and obtain

$$\int_R^1 dr r^2 v_{nk}(r)v_{n'k'}(r) = \frac{v_{nk}(1)v_{n'k'}(1)}{(\lambda_{nk}-\lambda_{n'k'})^2}\big([(\lambda_{nk}+\lambda_{n'k'}+2h^2) - 2h - 2nn'] - [(\lambda_{nk}+\lambda_{n'k'}+2h^2)R - 2h - 2nn'/R]\xi_{nk}\xi_{n'k'}\big). \tag{19}$$

In the limit $R\to 0$, the second term vanishes, yielding the results of Ref. 1 for the unit disk. A numerical determination of the solutions α_{nk} of Eq. (15) for given h and R allows one to construct the matrices Λ and $\mathcal{B}$ and the vectors U and $\tilde{U}$ through the above exact and explicit formulas.[23] After this preliminary step, the computation of the macroscopic signal is straightforward, rapid, and accurate.

B. Spherical layer

The above analysis can almost directly be applied to a spherical layer (or shell) $\Omega = \{\mathbf{r}\in\mathbb{R}^3 : R<|\mathbf{r}|<1\}$. In fact, the radial part $\tilde{v}(r)$ of the eigenfunctions satisfies a modified Bessel equation

$$r^2\tilde{v}'' + 2r\tilde{v}' + (\alpha^2 r^2 - n(n+1))\tilde{v} = 0. \quad (20)$$

A general solution of this equation is a linear combination of the spherical Bessel functions of the first and second kinds,

$$\tilde{v}(r) = c^{(1)} j_n(\alpha r) + c^{(2)} y_n(\alpha r),$$

which are defined as

$$j_n(z) = \sqrt{\frac{\pi}{2z}} J_{n+1/2}(z), \quad y_n(z) = \sqrt{\frac{\pi}{2z}} Y_{n+1/2}(z). \quad (21)$$

The Robin boundary conditions (14) remain unchanged, and the form of the equation for the parameter α is the same:

$$[\alpha j_n'(\alpha R) - h j_n(\alpha R)][\alpha y_n'(\alpha) + h y_n(\alpha)] - [\alpha j_n'(\alpha) + h j_n(\alpha)][\alpha y_n'(\alpha R) - h y_n(\alpha R)] = 0. \quad (22)$$

As previously, for each n and $0<R<1$, this equation has an infinite set of the positive solutions α_{nk} that we distinguish by a pair of indices n and k. The eigenvalues are $\lambda_{nk}=\alpha_{nk}^2$, while the eigenfunctions are

$$u_{nk}(r,\theta) = \frac{\beta_{nk}}{\sqrt{2\pi}} \frac{\tilde{v}_{nk}(r)}{\tilde{v}_{nk}(1)} P_n(\cos\theta),$$

where $P_n(z)$ are the Legendre polynomials. Note that the dependence on the polar coordinate φ is omitted here since it would be factored out anyway after integration (under the assumption that the magnetic field does not depend on φ). The normalization coefficients are determined in Appendix A,[24]

$$\beta_{nk}^{-2} = \frac{\lambda_{nk} - n(n+1) - h + h^2}{(2n+1)\lambda_{nk}} - \frac{R(\lambda_{nk}R^2 - n(n+1) - h + Rh^2)\xi_{nk}^2}{(2n+1)\lambda_{nk}}, \quad (23)$$

where

$$\xi_{nk} = \frac{\tilde{v}_{nk}(R)}{\tilde{v}_{nk}(1)}.$$

For a linear magnetic-field gradient, $B(\mathbf{r})=r\cos\theta$, the integration over the angular coordinate yields

$$\mathcal{B}_{nk,n'k'} = \frac{(n+n'+1)\delta_{n,n'\pm 1}}{(2n+1)(2n'+1)} \times \frac{\beta_{nk}\beta_{n'k'}}{\tilde{v}_{nk}(1)\tilde{v}_{n'k'}(1)} \int_R^1 dr r^3 \tilde{v}_{nk}(r)\tilde{v}_{n'k'}(r). \quad (24)$$

The last integral is found in Appendix A:

$$\int_R^1 dr r^3 \tilde{v}_{nk}(r)\tilde{v}_{n'k'}(r) = \frac{\tilde{v}_{nk}(1)\tilde{v}_{n'k'}(1)}{(\lambda_{nk}-\lambda_{n'k'})^2}\Big(\big[(\lambda_{nk}+\lambda_{n'k'}) + 2(1-h)^2 - n(n+1) - n'(n'+1)\big] - \big[(\lambda_{nk}+\lambda_{n'k'})R^2 + 2(1-Rh)^2 - n(n+1) - n'(n'+1)\big]\xi_{nk}\xi_{n'k'}\Big). \quad (25)$$

As previously, one needs first to determine numerically the solutions of Eq. (22) in order to build the matrices $\mathcal{B}$ and Λ according to the above exact and explicit relations.

IV. THIN LAYERS

Many analytical results can be obtained for thin circular and spherical layers when the inner radius R is close to the outer radius 1 [Fig. 1(b)]. We focus on the two-dimensional case, but the analysis is readily applicable in three dimensions.

A. Perturbative analysis

In the limit $R\to 1$, one can perturbatively solve Eq. (15) determining the roots α and thus the eigenvalues and partly the elements of the matrix $\mathcal{B}$. It is worth noting that such a perturbative approach is applicable for boundaries without relaxation ($h=0$). In fact, two boundary conditions (14) can simultaneously be satisfied in the limit $R\to 1$ only for $h=0$. For this reason, we focus on the Neumann boundary condition in this section.

When $h=0$, the radial part of the eigenfunctions can be written as[25]

$$v_{nk}(r) = J_n(\alpha_{nk}r)Y_n'(\alpha_{nk}) - Y_n(\alpha_{nk}r)J_n'(\alpha_{nk}), \quad (26)$$

while Eq. (15) is reduced to

$$J_n'(\alpha R)Y_n'(\alpha) - J_n'(\alpha)Y_n'(\alpha R) = 0. \quad (27)$$

A solution α of this equation depends on R. Denoting the thickness $\ell=1-R$, we substitute a formal series expansion

$$\alpha = a_0 + a_1\ell + a_2\ell^2 + a_3\ell^3 + \ldots \quad (28)$$

into Eq. (27) and expand it into a power series of small parameter ℓ. Setting $\ell\to 0$, one obtains the equation for a_0

$$J_n''(a_0)Y_n'(a_0) - J_n'(a_0)Y_n''(a_0) = 0. \quad (29)$$

This equation has the unique positive solution $a_0=n$. The other coefficients a_i of the perturbative series (28) are found in Appendix B. The related eigenvalue α^2 is then

$$\lambda_{n0} = n^2\left(1 + \ell + \frac{5}{6}\ell^2 + \frac{2}{3}\ell^3 - \frac{(n^2-16)}{30}\ell^4 + O(\ell^5)\right). \quad (30)$$

Interestingly, the first three corrections are independent of n, while the fourth- and higher-order corrections exhibit such dependence. Note also that the lowest eigenvalue λ_{00} is strictly equal to 0 independently of ℓ, as it should be for Neumann boundary condition. The perturbative relation is accurate for a broad range of R (or ℓ), not only for R close to 1. For example, Eq. (30) gives λ_{10} at $R=0.5$ with accuracy better than 1%, as compared to a numerical resolution of Eq. (27).

Since Eq. (29) has the unique positive solution, the other roots α_{nk} (with $k>0$) of the original Eq. (27) should increase up to infinity in the limit $R\to 1$. The above perturbative analysis is thus not applicable to deal with Bessel functions

of large argument α. In Appendix C, we use the asymptotic behavior of Bessel functions to obtain the other positive solutions α_{nk} of Eq. (27) with $k>0$:

$$\alpha_{nk} = \frac{\pi k}{\ell} + \frac{n^2+3/4}{2\pi k}\frac{\ell}{R} + O(\ell^3). \tag{31}$$

The first term has a simple geometric interpretation in terms of the oscillating eigenfunctions $u_{nk}(r,\varphi)$. In fact, Eq. (16) tells us that the first index n counts the number of maxima or "bumps" of the eigenfunction $u_{nk}(r,\varphi)$ along the angular coordinate φ, while the index k does the same for the radial coordinate r. In turn, the typical size of each bump is of the order of $\lambda_{nk}^{-1/2}=\alpha_{nk}^{-1}$. When R is close to 1, the thickness ℓ of the circular layer is much smaller than its length 2π [Fig. 1(b)]. In order to allocate k bumps along the radial coordinate, their sizes should be of the order of ℓ/k, yielding Eq. (31). The "justification" of the factor π and the correction term needs more accurate analysis of Appendix C.

The computation of the matrix $\mathcal{B}$ requires also the knowledge of the function $v_{nk}(r)$ at the inner boundary $r=R$ or, more precisely, the ratio $\xi_{nk}=v_{nk}(R)/v_{nk}(1)$. For thin layers, we derive in Appendix B that

$$\xi_{n0} = 1 - \frac{n^2}{6}\ell^3 - \frac{n^2}{4}\ell^4 + O(\ell^5). \tag{32}$$

In turn, the asymptotic behavior of Bessel functions in Eq. (26) for large argument α_{nk} with $k>0$ yields (see Appendix C)

$$\xi_{nk} = \frac{(-1)^k}{\sqrt{R}} + O(\ell^3). \tag{33}$$

In summary, the set of Eqs. (30)–(33) completely determines the elements of the matrices $\mathcal{B}$ and Λ that govern the evolution of the magnetization in thin circular layers. This is a striking result since the analysis for the broad family of thin layers (with various inner radii R) turns out to be much simpler and more explicit than that for the unit disk.

The results for thin spherical layers (or shells) can be obtained in a very similar manner. In Appendix B, we show that

$$\lambda_{n0} = n(n+1)\left(1 + \ell + \frac{2}{3}\ell^2 + \frac{1}{3}\ell^3 - \frac{(3n(n+1)-10)}{90}\ell^4 + O(\ell^5)\right) \tag{34}$$

and

$$\xi_{n0} = 1 - \frac{n(n+1)}{6}\ell^3 - \frac{n(n+1)}{4}\ell^4 + O(\ell^5). \tag{35}$$

Both perturbative relations (34) and (35) give accurate results for a broad range of R. In Appendix C, we obtain α_{nk} (and thus λ_{nk}) and ξ_{nk} with $k>0$:

$$\alpha_{nk} = \frac{\pi k}{\ell} + \frac{n^2+n+2}{2\pi k}\frac{\ell}{R} + O(\ell^3) \tag{36}$$

and

$$\xi_{nk} = \frac{(-1)^k}{R} + O(\ell^3). \tag{37}$$

As previously, the set of Eqs. (34)–(37) completely determines the elements of the matrices $\mathcal{B}$ and Λ and thus the evolution of the magnetization in thin spherical layers.

B. Apparent diffusion coefficient

As mentioned in Sec. II, a theoretical analysis of restricted diffusion in NMR is often reduced to the study of the second moment $\mathbb{E}\{\phi^2/2\}$ which determines the macroscopic signal at weak gradients. If there is no surface relaxation ($h=0$), the ground eigenfunction $u_0(\mathbf{r})$ is constant, yielding $U_m=\tilde{U}_m=\delta_{m,0}$ for the uniform initial density $\rho(\mathbf{r})=1/V$ and constant pickup function $\tilde{\rho}(\mathbf{r})=1$. The general formula (12) can thus be written as

$$\mathbb{E}\{\phi^2/2\} = \langle \mathbb{E}\{B(X_{t_1})B(X_{t_2})\}\rangle_2, \tag{38}$$

where

$$\mathbb{E}\{B(X_{t_1})B(X_{t_2})\} = \sum_{nk} \mathcal{B}_{00,nk} e^{-p\lambda_{nk}(t_2-t_1)} \mathcal{B}_{nk,00}, \tag{39}$$

and we define the f-weighted time average $\langle\cdots\rangle_2$ for any function $F(t_1,t_2)$ of two variables t_1 and t_2 as

$$\langle F(t_1,t_2)\rangle_2 = \int_0^1 dt_1 f(t_1) \int_{t_1}^1 dt_2 f(t_2) F(t_1,t_2).$$

The second moment is directly related to the effective, time-dependent or, equivalently, apparent diffusion coefficient (ADC),[26]

$$D(p) = D\frac{\mathbb{E}\{\phi^2/2\}}{p\langle(t_1-t_2)\rangle_2}, \tag{40}$$

where p stands here instead of diffusion time: $p=DT/L^2$. The denominator is chosen to get $D(0)=D$ as expected. According to Eq. (39), the ADC is expressed as the following sum:

$$\frac{D(p)}{D} = \sum_{k=0}^{\infty} \lambda_{1k}\mathcal{B}_{00,1k}^2 w(p\lambda_{1k}), \tag{41}$$

where the sum over n was reduced to $n=1$ due to Kronecker symbol in Eq. (18), and the function $w(p)$ depends only on the choice of the temporal profile $f(t)$:

$$w(p) = \frac{\langle e^{-p(t_2-t_1)}\rangle_2}{p\langle(t_1-t_2)\rangle_2}.$$

This function approaches 1 for small p and behaves as p^{-2} for large p. For instance, if $f(t)$ is a bipolar rectangular profile,

$$f(t) = \Theta(t) - 2\Theta(t-1/2) + \Theta(t-1) \tag{42}$$

[here $\Theta(t)$ is the Heaviside step function: $\Theta(t)=1$ for $t>0$ and 0 otherwise], one finds $\langle(t_1-t_2)\rangle_2=1/12$ and

$$w(p) = 12\left(\frac{1}{p^2} - \frac{e^{-p}-4e^{-p/2}+3}{p^3}\right). \tag{43}$$

Note also that the function $w(p)$ is defined to get[1]

$$\sum_{k=0}^{\infty} \lambda_{1k} \mathcal{B}_{00,1k}^2 = 1.$$

This means that each term $\lambda_{1k}\mathcal{B}_{00,1k}^2$ can be thought of as a weight of the eigenfunction u_{1k} contributing to ADC. In turn, the eigenvalue λ_{1k} determines a characteristic scale at which the contribution appears in Eq. (41) through the function $w(p)$. The formulas (18) and (24) allow one to calculate the weights in circular or spherical layers, respectively.

The analysis can further be simplified in the limit of thin layers. For the sake of simplicity, we restrict ourselves to the second-order perturbative analysis in small parameter ℓ. The crucial simplification relies on the fact that the eigenvalues λ_{1k} with $k>0$ are much larger than λ_{10}. In fact, the eigenvalue λ_{10} is close to 1 for circular layers and 2 for spherical layers according to Eqs. (30) and (34), while the others behave like $\pi^2 k^2/\ell^2$ due to Eqs. (31) and (36). Standing in the argument of the exponential function in Eq. (39), the large eigenvalues make these terms small,[27] expect for very small p. Given that $\xi_{10}=1+O(\ell^3)$, one calculates $\lambda_{10}\mathcal{B}_{00,10}^2$ for a linear gradient profile and gets particularly simple formulas for ADC for large enough p in the cases of cylindrical ($d=2$) and spherical ($d=3$) shells, respectively:

$$D(p)/D \simeq \left(\frac{2}{\lambda_{10}(1+R)^2}\right) w(p\lambda_{10}),$$
$$D(p)/D \simeq \left(\frac{2(1-R^2)^2}{(1-R^3)[\lambda_{10}(1-R^3)-2(1-R)]}\right) w(p\lambda_{10}), \tag{44}$$

where λ_{10} is given by Eq. (30) in 2D and Eq. (34) in 3D. The expressions in parentheses, depending only on R, approach, respectively, $1/2$ and $2/3$ as R going to 1. The ratio $2/3$ has a simple intuitive explanation: 3D diffusion in a thick spherical shell is reduced to essentially 2D motion in a thin spherical shell. Similarly, 2D diffusion in a thick circular layer (a 2D shape) is reduced to one-dimensional motion in a thin circular layer, yielding the reduction factor $1/2$. When these arguments are applied to a cylindrical shell (a 3D object), one may expect to retrieve again the ratio $2/3$, as for a spherical shell. This "puzzle" is fully resolved by recalling that $D(p)/D$ is probed by NMR, when restricted diffusion is "seen" along a given gradient direction. When the gradient is perpendicular to the cylinder axis, displacements of the spin-bearing particles along this axis do not attenuate the spin-echo signal, and diffusion can be seen as a two-dimensional process in a circular layer. In this perspective, all the results deduced here for circular layers can be applied to cylindrical shells.

We recall that this result is valid for thin circular and spherical layers (small ℓ) without surface relaxation ($h=0$) assuming that p is not too small. It is worth stressing that the limits $\ell \to 0$ and $p \to 0$ cannot be exchanged. Actually, in the limit $p \to 0$, all eigenvalues λ_{1k}, both with $k=0$ and $k>0$, intervene and contribute to the macroscopic signal. A general analysis of this slow-diffusion regime was given in Refs. 1–4.

C. Discussion

The apparent diffusion coefficient depends directly on the diffusion time T through the dimensionless parameter p defined as square of the ratio between the diffusion length $\sqrt{DT}$ and a typical geometrical scale L. It is thus natural to expect two different regimes for $\sqrt{DT} \ll L$ (or $p \ll 1$) and $\sqrt{DT} \gg L$ (or $p \gg 1$). In the former so-called "slow-diffusion regime," only a small fraction of particles near the boundary can "feel" the confinement. In particular, the second moment is proportional to p as for free diffusion, with the $p^{3/2}$ and higher-order corrections accounting for boundary effects. In the opposite limit $p \gg 1$, the behavior depends on whether the confining domain is bounded or not. In "motional-narrowing regime," every particle has enough time to explore the whole bounded domain, and the second moment is proportional to $1/p$ (with p^{-2} and higher-order corrections). In turn, if the medium is unbounded (but statistically homogeneous and isotropic), the confinement results in slower diffusive transport which is characterized by a constant ADC smaller than D.[4,28–30] The ratio between free diffusion coefficient D and ADC, the tortuosity, is an important characteristic of porous media. In this "tortuosity regime," the second moment is again proportional to p. Each of these diffusion regimes has been thoroughly investigated by theoretical, numerical, and experimental methods (see reviews[1,4] and references therein).

The choice of a typical geometrical scale L is ambiguous for multiscale structures. In this paper, we took $L=1$, the outer radius of the layer. However, the presence of the second geometrical scale, the thickness ℓ of the layer, and its smallness with respect to L for thin layers favor the possibility for a new, intermediate regime when $\ell \ll \sqrt{DT} \ll L$. This means that one can choose the diffusion time T long enough for particles to travel between two boundaries but still insufficient for exploring the whole domain. This situation resembles tortuosity regime, although thin layers are neither homogeneous nor statistically isotropic. Nonetheless, the use of thin layers as simplified confinements allows one to investigate, for the first time, successive transitions between three aforementioned diffusion regimes in a single mathematical frame.

This transition is illustrated in Fig. 2 showing the normalized apparent diffusion coefficient $D(p)/D$ as a function of p for a thick and a thin circular layers with the inner radii $R=0.5$ and $R=0.9$, respectively. For the first domain, the thickness $\ell=0.5$ does not much differ from the outer radius $L=1$ (or also length 2π), so that the scale window $0.25 \ll p \ll 1$ (shown by vertical dashed lines) for the intermediate regime is too narrow. In this case, one observes a mere transition between slow-diffusion and motional-narrowing regimes, as for the unit disk. In contrast, the behavior of ADC for a thin layer is sharply different. Since the thickness $\ell=0.1$ is significantly smaller than $L=1$, the scale window $0.01 \ll p \ll 1$ is large enough to reveal the new intermediate regime. At this time and length scale, the restricted diffusion in a two-dimensional thin layer is effectively one dimensional so that the apparent diffusion coefficient is reduced by factor 2. This reduction factor can formally be interpreted as

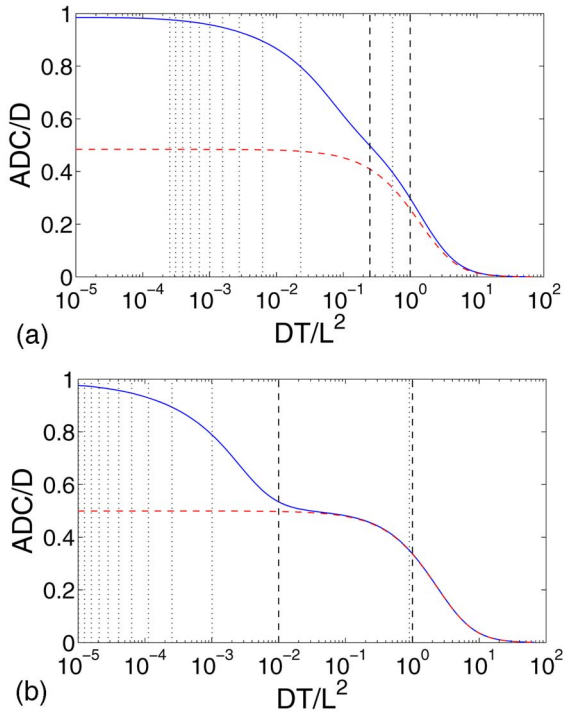

FIG. 2. (Color online) Normalized apparent diffusion coefficient $D(p)/D$ as a function of the dimensionless parameter p for circular layers with inner radii $R=0.5$ (top) and $R=0.9$ (bottom). The solid line shows the exact computation via Eq. (41), while the dashed line represents the approximate solution (44) containing only the first contributing eigenvalue λ_{10} and thus failing for small p. Two vertical dashed lines (at ℓ^2 and 1) roughly split the p axis in three regions: slow-diffusion regime (on the left, $p \ll \ell^2$), intermediate region, and motional-narrowing regime (on the right, $p \gg 1$). The vertical dotted lines show the scales λ_{1k}^{-1} (k ranging from 0 to 10, with $k=0$ on the right and $k=10$ on the left). One can observe a plateau due to a large separation between the two contributing eigenvalues λ_{10} and λ_{11} (thinner the layer, wider the plateau).

the tortuosity of a thin layer. Note that this tortuosity is almost independent of the thickness ℓ, given that ℓ is small. A complete analytical description developed in this paper allows to study first the transition from the slow diffusion to the intermediate (or tortuosity) regime at p around ℓ^2, and then the transition to the ultimate motional-narrowing regime when p exceeds 1. As expected, the thinner the layer, the larger the scale window for the intermediate regime.

The above consideration was essentially based upon scaling arguments. In particular, the frontiers ℓ^2 and 1 of the scale window for the intermediate regime are vague. These arguments can be put in rigorous mathematical terms with the help of the MCF matrix formalism involving Laplace operator eigenbasis, as shown below.

In NMR, restricted diffusion is monitored by applying a time-dependent spatially inhomogeneous magnetic field. Choosing a linear gradient for the spatial profile makes the eigenmodes with $n=1$ to be the only contributing eigenmodes to the second moment and, consequently, the apparent diffusion coefficient. In turn, the temporal profile $f(t)$ fixes the function $w(p)$, a kind of elementary contribution to ADC. In particular, $D(p)$ is obtained as the weighted sum of these contributions at scales λ_{1k}. Since the first two scales λ_{10} and λ_{11} are largely separated, one can choose p satisfying $\lambda_{11}^{-1} \ll p \ll \lambda_{10}^{-1}$, for which $w(p\lambda_{10})$ is almost constant, while $w(p\lambda_{1k})$ for $k>0$ are still small. As a consequence, the ADC exhibits a plateau for these values of p, as shown in Fig. 2. The eigenvalues λ_{10} and λ_{11} determine thus the scale window for the intermediate regime. Since $\lambda_{10}^{-1} \simeq 1$ and $\lambda_{11}^{-1} \simeq \ell^2/\pi^2$, the rigorous bounds are close to the previous scaling bounds 1 and ℓ^2, respectively. It is worth noting that the limits of the scale window cannot be sharp anyway since the function $w(p)$ is rather extended.

One may also wonder whether the intermediate regime with a reduced but constant ADC emerges whenever the separation in length scales occurs. As we have seen for thin layers, the distinction between the thickness ℓ and the perimeter $2\pi L$ results in a large gap between the eigenvalues $\lambda_{n0} \simeq n^2$ and $\lambda_{nk} \simeq \pi^2 k^2/l^2$ with $k>0$. The former eigenvalues λ_{n0} describe large displacements in angular coordinates along the boundaries (i.e., along the circumference of the circular layer), while the latter eigenvalues λ_{nk} correspond to small displacements in radial coordinate (i.e., perpendicular to the boundaries). In the above leading-term approximation, the first set of eigenvalues can formally be associated with diffusion on the interval $[0,\pi]$, corresponding to a half-circle[33] of radius $L=1$. In turn, the eigenvalues λ_{nk} with $k>0$ (for any n) are associated with diffusion on the interval $[0,\ell]$ corresponding to motion between the inner and outer boundaries. This situation is somehow analogous to restricted diffusion in a thin rectangle with sides π and ℓ. For this simple domain, one has $\lambda_{nk}=n^2+\pi^2k^2/\ell^2$, so that $\lambda_{n0}=n^2$ for $k=0$ and $\lambda_{nk} \simeq \pi^2k^2/\ell^2$ for $k>0$, as for thin layers. As shown in Appendix D, the matrix $\mathcal{B}$ is also split in two parts, yielding a decomposition of the ADC in two separate contributions corresponding to one-dimensional restricted diffusions along the two sides. However, in sharp contrast with thin layers, an intermediate regime with a constant ADC does not emerge for a rectangular domain since the eigenmodes with any n do contribute. In turn, the rotation invariance of the circular (and spherical) layers eliminates the contributions of all eigenmodes except for $n=1$. This comparison clearly shows that the presence of multiple scales is important but insufficient condition for observing the intermediate diffusion regime with a constant ADC. A kind of isotropy is also required.

In general, a significant separation in length scales in statistically homogeneous and isotropic porous media is expected to result in distinct regions of constant ADCs. Since these regions can in principle[34] be observed by varying the diffusion time T (and thus p), one may have an experimental tool for detecting multiple scales. However, a reliable interpretation of such measurements still requires a substantial study of the Laplace operator eigenbasis in porous structures. The present work can only be considered as a first step toward a better theoretical understanding of these features in multiscale porous structures.

Similar arguments and results hold for thin spherical layers. So, restricted diffusion in these three-dimensional domains is effectively two dimensional, yielding the reduction of diffusion coefficient by factor 2/3. A constant region in the dependence of $D(p)$ on p (not presented) is very similar to that shown in Fig. 2.

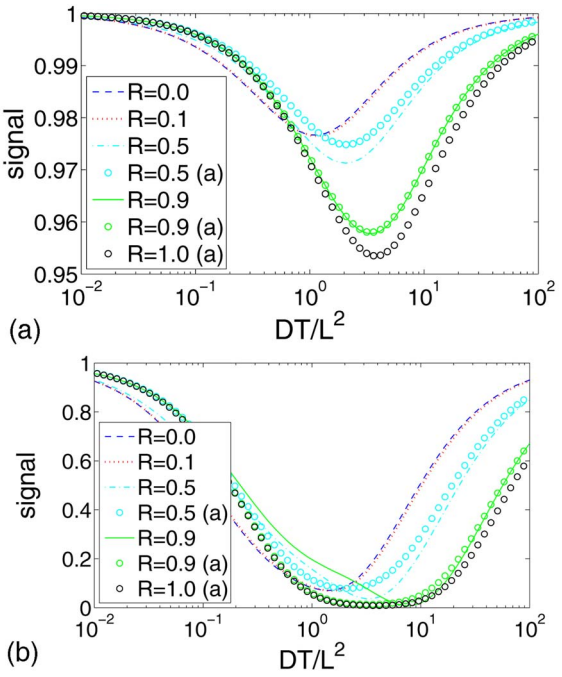

FIG. 3. (Color online) Spin-echo signal at two values $q=1$ (top) and $q=10$ (bottom) of the dimensionless gradient intensity $q=\gamma gLT$ as a function of the dimensionless parameter $p=DT/L^2$ for circular layers with various inner radii R. The lines represent the results of numerical computation by the matrix formalism of Sec. II, while the circles show approximate theoretical behavior obtained by a combined use of Eqs. (11), (30), (44), and (43). For all cases, the bipolar rectangular temporal profile (42) is used.

D. Beyond the Gaussian-phase approximation

Although the apparent diffusion coefficient can always be introduced by Eq. (40) through the second moment, its relation (11) to the macroscopic signal holds only for weak gradients (small q). When the gradient is large enough, the higher-order moments become significant, and the above Gaussian-phase approximation fails.[35–37] Using the MCF-based technique, one can still calculate the macroscopic signal numerically even in this case. We consider circular layers with various inner radii and compute the macroscopic signal as a function of p for two values of the dimensionless intensity: $q=1$ and $q=10$ (Fig. 3). In both cases, the signal approaches 1 in the slow-diffusion ($p \ll 1$) and motional-narrowing ($p \gg 1$) regimes, the minimum being reached for an intermediate value of p. When the thickness of the layer decreases, the minimum is getting deeper (smaller signal), and its position is shifted toward larger p. It is worth stressing that here there is no surface relaxation ($h=0$), the signal attenuation is purely related to spin dephasing in a linear magnetic-field gradient of the same intensity. As expected, the attenuation is much more pronounced for $q=10$ as compared to $q=1$.

For circular layers with $R=0.5$ and $R=0.9$, the numerically computed signals (shown by lines) are compared to that given by Gaussian-phase approximation (11) (shown by circles), where the second moment is expressed through Eqs. (40) and (44). In the former case $R=0.5$, one observes deviations, independently of q, because the perturbative analysis is not accurate for $\ell=0.5$ [i.e., the approximation (44) fails]. In this respect, the case of a thin layer with $R=0.9$ is much more interesting. For $q=1$, the approximation works correctly, accurately reproducing the numerical signal. However, for $q=10$, the Gaussian-phase approximation (11) fails, yielding large deviations due to the high-order moments. Note that similar results were observed for spherical layers (not shown). Although our perturbative description for thin layers allows for a detailed study of the higher-order moments and the consequent non-Gaussian behavior, this topic goes beyond the scope of the present paper.

V. CONCLUSIONS

In this paper, we presented a mathematical description and thorough study of restricted diffusion in circular and spherical layers. This analysis relies on a recently developed matrix formalism relating the macroscopic signal, attenuated in the presence of inhomogeneous magnetic fields and surface relaxation, to the matrices $\mathcal{B}$ and Λ involving the Laplace operator eigenbasis. For linear gradient and parabolic magnetic fields, we derived exact analytical formulas for the elements of the matrix $\mathcal{B}$, allowing for a rapid and very accurate numerical computation of the macroscopic signal for any temporal profile (waveform) $f(t)$ of the magnetic field. This is a considerable extension of our previous results for the unit disk and sphere.

When the thickness ℓ of a layer is small with respect to its overall size, the elements of the matrices $\mathcal{B}$ and Λ have been determined explicitly as perturbative series in powers of ℓ. Surprisingly, the case of thin layers is not only richer but also much simpler than that of the unit disk or sphere, which were repeatedly invoked in the literature as basic confining domains. The particular interest in studying thin layers is that these are the shapes with two different geometrical scales (thickness and overall size), for which a rigorous analytical study is still feasible. The two-scale character is explicitly reflected in the properties of the underlying Laplace operator eigenbasis. So, the eigenvalues λ_{nk} exhibit drastically different behaviors for $k=0$ and $k>0$, describing, respectively, large displacements along the boundary and small displacements perpendicular to the boundary. The separation in length scales can be revealed through the behavior of the time-dependent apparent diffusion coefficient. When the diffusion length lies between two geometrical scales, one faces an intermediate diffusion regime with a nearly constant ADC. This is a new, two-scale feature which could not be observed for one-scale domains such as the unit disk or sphere. In practice, the emergence of such a region in the dependence of ADC as a function of diffusion time would be a sign of a two-scale or, in general, multiscale geometry. A thorough numerical analysis of the Laplace operator eigenbasis in multiscale porous media would further extend our knowledge about restricted diffusion in NMR.

ACKNOWLEDGMENTS

This work has been supported by the ANR projects "MIPOMODIM" and "DYOPTRI."

APPENDIX A: ANALYTICAL COMPUTATION OF THE MATRIX $\mathcal{B}$

Analytical computation of the integrals involving Bessel functions can often be reduced to algebraic operations with Bessel equation and integration by parts. In particular, the analytical form for the elements of the matrix $\mathcal{B}$ is derived in this elementary though tricky way. Since these expressions have not been found in the literature, we present here the main steps of their calculation. Although this part is technical, this is an important mathematical basis for the present and further studies of restricted diffusion in rotation-invariant domains.

1. Basic idea

We denote $v(r)$ a solution of the Bessel equation:

$$(rv')' + (\alpha^2 r - \nu^2/r)v = 0, \tag{A1}$$

where α and ν are two real positive numbers. In general, $v(r)$ is a linear combination of two independent solutions $J_\nu(\alpha r)$ and $Y_\nu(\alpha r)$ which are called, respectively, Bessel functions of the first and second kinds of order ν.[21,22,38] Here, we do not restrict ν to take integer values (as it should be for circular layers), bearing in mind the application to spherical layers for which the solution involves Bessel functions with half-integer indices.

First, we illustrate the basic idea by computing the normalization coefficients β_{nk} of the eigenfunctions. This is a classical procedure which can be found in any textbook on mathematical physics. For a circular layer with inner and outer radii a and b, one needs to calculate the following integral:

$$\int_a^b dr r v^2(r). \tag{A2}$$

The application of standard integration tools for a direct computation of this integral is difficult, but a simple use of the Bessel equation makes it elementary. In fact, the multiplication of Eq. (A1) by (rv') and its integration over $[a,b]$ gives

$$\begin{aligned} 0 &= \int_a^b dr[(rv')' + (\alpha^2 r - \nu^2/r)v](rv') \\ &= \frac{1}{2}\int_a^b dr[([rv']^2)' + \alpha^2 r^2 (v^2)' - \nu^2 (v^2)']. \end{aligned}$$

Integration by parts yields

$$\int_a^b dr r v^2 = \frac{1}{2\alpha^2}\left(r^2 (v')^2 + [\alpha^2 r^2 - \nu^2]v^2\right)_a^b. \tag{A3}$$

In the right-hand side, we use the standard notation, meaning the difference between two values of the primitive (the expression in the big parentheses) at the upper and lower integral limits $r=b$ and $r=a$. The substitution of $v'(r)$ at $r=a=R$ and $r=b=1$ from the boundary conditions (14) leads to Eq. (17) for the normalization coefficients β_{nk}.[39]

2. General case

The very same idea can directly be applied to compute the integrals involving the solutions of two different Bessel equations. In this section, we consider the following integral:

$$\int_a^b dr r^k v_1 v_2, \tag{A4}$$

where k is a positive integer, and $v_1(r)$ and $v_2(r)$ satisfy two Bessel equations (A1) with $\alpha_1 \neq \alpha_2$ (while the indices ν_1 and ν_2 may be equal or not). For instance, the integral (A4) with $k=2$ determines the elements of the matrix $\mathcal{B}$ for a linear magnetic-field gradient in a circular layer.

Standard integration tools for a direct computation of the integral (A4) are barely useful. We propose the following roundabout trick. As previously, we would like first to use Bessel equations to replace functions v_1 and v_2 by their derivatives and then to integrate the result by parts. For this purpose, we multiply the integral (A4) by α_1^2 and α_2^2 acting on v_1 and v_2 as a kind of radial Laplace operator. More precisely, we consider

$$I \equiv (\alpha_1^2 - \alpha_2^2)^2 \int_a^b dr r^k v_1 v_2.$$

The computation of this integral is based on successive use of the Bessel equation and integration by parts. We skip lengthy intermediate steps and give the final result

$$\begin{aligned} I = &\left((\alpha_1^2 + \alpha_2^2)(k-1) r^{k-1} v_1 v_2 + (\alpha_1^2 - \alpha_2^2) r^k (v_1 v_2' - v_1' v_2) + 2(k-1) r^{k-1} v_1' v_2' - (\nu_1^2 - \nu_2^2 - (k-1)^2) r^{k-2} v_1' v_2 \right. \\ &\left. - (\nu_2^2 - \nu_1^2 - (k-1)^2) r^{k-2} v_2' v_1 \right)_a^b + \left[(\nu_1^2 - \nu_2^2 - (k-1)^2)(k-3) - 2(k-1)\nu_1^2\right] \int_a^b dr r^{k-3} v_2' v_1 + \left[(\nu_2^2 - \nu_1^2 - (k-1)^2)(k-3)\right. \\ &\left. - 2(k-1)\nu_2^2\right] \int_a^b dr r^{k-3} v_1' v_2 - 4(k-1)(k-2) \int_a^b dr r^{k-2} v_1' v_2' + \left[(\nu_1^2 - \nu_2^2)^2 - (k-1)^2(\nu_1^2 + \nu_2^2)\right] \int_a^b dr r^{k-4} v_1 v_2. \end{aligned} \tag{A5}$$

At first thought, this cumbersome expression appears to be useless since the integral (A4) is expressed through several other integrals. Under certain conditions, however, this expression becomes considerably simpler. It is rather fortunate that these conditions are fulfilled in the cases of practical interest such as a linear gradient or even parabolic magnetic field. As shown below, Eq. (A5) leads to a closed explicit relation for the integral (A4) in these particular cases.

3. Linear gradient in circular layer

For a linear gradient in circular layers, Eq. (18) for the elements of the matrix $\mathcal{B}$ requires the computation of the integral (A4) with $k=2$, under the condition $|\nu_1-\nu_2|=1$ coming after the integration over the angular coordinate. In this case, the general result (A5) can be reduced, after integration by parts, to a closed explicit formula. The use of the boundary conditions (14) completes the derivation of Eq. (19). We stress that this result is exact; no simplifying assumption or approximation was employed. On the other hand, the condition $|\nu_1-\nu_2|=1$ was crucial: if the angular part of the linear gradient was different (e.g., $r\cos 2\varphi$ instead of $r\cos\varphi$), no explicit relation could probably be derived for the elements of the matrix $\mathcal{B}$.

4. Parabolic field in circular layer

Although less important for practical applications, the parabolic spatial profile $B(\mathbf{r})=|\mathbf{r}|^2=r^2$ is often considered as a paradigm of a nonlinear magnetic field.[40] In this case, the computation of the elements of the matrix $\mathcal{B}$ involves the integral (A4) with $k=3$ (see Ref. 1 for details). The isotropic character of the parabolic field and the rotation invariance of the domain lead to $\nu_1=\nu_2=n$ after integration over the angular coordinate

$$\mathcal{B}_{nk,n'k'}=2\delta_{n,n'}\frac{\beta_{nk}\beta_{n'k'}}{v_{nk}(1)v_{n'k'}(1)}\int_1^R drr^3v_{nk}(r)v_{n'k'}(r).$$

Without showing technical details, we give the net result obtained from Eq. (A5) in this case

$$\int_a^b drr^3v_1v_2=\frac{2}{(\alpha_1^2-\alpha_2^2)^2}\big([(\alpha_1^2+\alpha_2^2+2h^2)\times r^2-2n^2]v_1v_2\big)_a^b,$$

where we used boundary conditions (14). In a similar way, one can explicitly calculate the integral

$$\int_a^b drr^3v^2=\frac{1}{6}\left(r^4v^2+\frac{1}{\alpha^2}[n^2r^2v^2-2r^3v'v+r^4(v')^2]+2\frac{n^2-1}{\alpha^4}[r^2(v')^2-n^2v^2]\right)_a^b, \tag{A6}$$

determining the diagonal elements of the matrix $\mathcal{B}$ for the parabolic magnetic field.

5. Application to spherical layers

The result (A5) is also applicable in the case of spherical layers. We first recall that the spherical Bessel functions $j_n(z)$ and $y_n(z)$ are related to Bessel function with half-integer indices according to Eq. (21). As a consequence, any linear combination $\tilde{v}(r)$ of the spherical Bessel functions satisfies Eq. (20) and can be represented as

$$\tilde{v}(r)=\sqrt{\frac{\pi}{2\alpha}}\frac{v(r)}{\sqrt{r}},$$

where $v(r)$ is the linear combination of the corresponding Bessel functions with half-integer indices $\nu=n+1/2$. So, the formulas (23) and (25) for the normalization coefficients β_{nk} and for the elements of the matrix $\mathcal{B}$ in the case of a linear gradient were obtained by "translating" the previous results for $v(r)$ into new ones for $\tilde{v}(r)$.

For a parabolic magnetic field, the matrix $\mathcal{B}$ is[41]

$$\mathcal{B}_{nk,n'k'}=\frac{2\delta_{n,n'}}{2n+1}\frac{\beta_{nk}\beta_{n'k'}}{\tilde{v}_{nk}(1)\tilde{v}_{n'k'}(1)}\int_R^1 drr^4\tilde{v}_{nk}(r)\tilde{v}_{n'k'}(r),$$

where

$$\int_a^b drr^4\tilde{v}_1\tilde{v}_2=\frac{2}{(\alpha_1^2-\alpha_2^2)^2}\big(r[(\alpha_1^2+\alpha_2^2+2h^2)r^2-2hr-2n(n+1)]\tilde{v}_1\tilde{v}_2\big)_a^b$$

and

$$\int_a^b drr^4\tilde{v}^2=\frac{1}{6}\left(r^5\tilde{v}^2+\frac{1}{\alpha^2}[(n(n+1)-1/2)r^3\tilde{v}^2-r^4\tilde{v}'\tilde{v}+r^5(\tilde{v}')^2]+\frac{(2n-1)(2n+3)}{2\alpha^4}\times[r^3(\tilde{v}')^2+r^2\tilde{v}\tilde{v}'-n(n+1)r\tilde{v}^2]\right)_a^b,$$

determining the diagonal elements of the matrix $\mathcal{B}$ for the parabolic magnetic field.

APPENDIX B: PERTURBATIVE ANALYSIS FOR THIN LAYERS

In this appendix, we explain the main steps of a perturbative analysis of Eq. (27) in the limit $R\to 1$. A solution α of this equation can be considered as a perturbation series (28) in small parameter ℓ. This representation is substituted in Eq. (27) and the Bessel functions are in turn expanded into power series. This expansion involves the values of the Bessel functions J_n and Y_n and their multiple derivatives evaluated at a_0. In fact, the computation of α up to the correction $O(\ell^k)$ requires finding the derivatives of all orders up to $(k+1)$. Using the Bessel equation (13), one can first express the second-order derivative $J_n^{(2)}(z)$ in terms of $J_n(z)$ and $J_n'(z)$ as

$$J_n^{(2)}(z)=-\frac{(z^2-n^2)}{z^2}J_n(z)-\frac{1}{z}J_n'(z).$$

To calculate the third-order derivative, one differentiates this relation and then substitutes the above formula for $J_n^{(2)}(z)$:

$$J_n^{(3)}(z)=\frac{z^2-3n^2}{z^3}J_n(z)-\frac{z^2-n^2-2}{z^2}J_n'(z).$$

In this way, the derivative of any order can be iteratively expressed in terms of $J_n(z)$ and $J_n'(z)$. Similar relations hold for the Bessel function $Y_n(z)$. As a consequence, the pertur-

bation series for Eq. (27) contains four products $J_n(a_0)Y_n(a_0)$, $J_n'(a_0)Y_n(a_0)$, $J_n(a_0)Y_n'(a_0)$, and $J_n'(a_0)Y_n'(a_0)$ with complicated coefficients. The antisymmetric form of this equation leads to cancellation of the symmetric terms so that the first and the last products disappear. Moreover, the second and third products always enter with opposite signs. The perturbation series has thus the form

$$[J_n'(a_0)Y_n(a_0) - J_n(a_0)Y_n'(a_0)](A_1(a_0)\ell + A_2(a_0,a_1)\ell^2 + \dots) = 0, \tag{B1}$$

where A_j are explicitly derived combinations of a_j, e.g.,

$$A_1 = \frac{a_0^2 - n^2}{a_0},$$

$$A_2 = \frac{a_0^3 + 4a_1n^2 - 3a_0n^2}{2a_0^2}, \dots .$$

Since the left-hand side of Eq. (B1) should be equal to 0 for any ℓ, all combinations A_j must be 0, providing the successive equations for finding the coefficients a_0, a_1, a_2, etc. The net result of this computation is

$$\alpha_{n0} = n\left(1 + \frac{1}{2}\ell + \frac{7}{24}\ell^2 + \frac{3}{16}\ell^3 + \left(\frac{751}{5760} - \frac{n^2}{60}\right)\ell^4 + O(\ell^5)\right).$$

Taking the square of this perturbative expression, one gets Eq. (30). It is worth stressing that this analysis was carried out for the case without surface relaxation ($h=0$).

In addition, we calculate the value of the radial dependence $v(r)$ of the eigenfunctions at $r=R$. When $h=0$, the function $v(r)$ is given by Eq. (26) which has the similar structure as the previously considered Eq. (27). Using similar perturbative analysis, one obtains

$$v_{n0}(R) = \frac{2}{\pi n}\left(1 - \frac{1}{2}\ell - \frac{1}{24}\ell^2 - \frac{8n^2+1}{48}\ell^3 - \frac{3(32n^2+3)}{640}\ell^4 + O(\ell^5)\right),$$

where the prefactor $2/(\pi n)$ comes from the Abel's identity for Bessel functions at $z=a_0=n$:

$$J_n(z)Y_n'(z) - Y_n(z)J_n'(z) = \frac{2}{\pi z}.$$

This identity also implies that $v_{n0}(1)=2/(\pi\alpha_{n0})$, from which one deduces formula (32) for the ratio $\xi_{n0}=v_{n0}(R)/v_{n0}(1)$.

Similar perturbative analysis for thin spherical layers gives

$$\alpha_{n0} = \sqrt{n(n+1)}\left(1 + \frac{1}{2}\ell + \frac{5}{24}\ell^2 + \frac{1}{16}\ell^3 - \left(\frac{n(n+1)}{60} - \frac{1}{384}\right)\ell^4 + O(\ell^5)\right),$$

from which Eq. (34) was deduced. One also obtains

$$\tilde{v}_{n0}(R) = \frac{1}{n(n+1)}\left(1 - \ell + \frac{1}{3}\ell^2 - \frac{n(n+1)}{6}\ell^3 - \frac{n(n+1)}{20}\ell^4 + O(\ell^5)\right),$$

where the prefactor is given by Abel's identity for the spherical Bessel functions at $z=a_0=\sqrt{n(n+1)}$:

$$j_n(z)y_n'(z) - y_n(z)j_n'(z) = \frac{1}{z^2}.$$

This identity also implies $\tilde{v}_{n0}(1)=1/(\alpha_{n0}^2)$, from which one gets Eq. (35).

APPENDIX C: ASYMPTOTIC ANALYSIS FOR THIN LAYERS

In this appendix, we are looking for large solutions α of Eq. (27) which could not be obtained by the perturbative analysis of Appendix B. For large argument, Bessel functions exhibit the following asymptotic behavior[42]

$$J_\nu(z) = \sqrt{\frac{2}{\pi z}}\left[\cos\left(z - \frac{\pi}{2}\nu - \frac{\pi}{4}\right)P_\nu^1(z) - \sin\left(z - \frac{\pi}{2}\nu - \frac{\pi}{4}\right)P_\nu^2(z)\right],$$

$$Y_\nu(z) = \sqrt{\frac{2}{\pi z}}\left[\sin\left(z - \frac{\pi}{2}\nu - \frac{\pi}{4}\right)P_\nu^1(z) + \cos\left(z - \frac{\pi}{2}\nu - \frac{\pi}{4}\right)P_\nu^2(z)\right], \tag{C1}$$

with two polynomial in powers of $1/z$:

$$P_\nu^1(z) = \sum_{k=0}^{K-1}\frac{(-1)^k}{(2z)^{2k}}\frac{\Gamma(\nu+2k+1/2)}{(2k)!\Gamma(\nu-2k+1/2)} + O(z^{-2K}),$$

$$P_\nu^2(z) = \sum_{k=0}^{K-1}\frac{(-1)^k}{(2z)^{2k+1}}\frac{\Gamma(\nu+2k+3/2)}{(2k+1)!\Gamma(\nu-2k-1/2)} + O(z^{-2K-1})$$

(K determining the order of correction). From these relations, one can deduce the asymptotic behavior for the derivatives J_ν' and Y_ν'. Their substitution in Eq. (27) yields the explicit equation for α:

$$\sin\alpha(1-R)[Q_n^1(\alpha)Q_n^1(\alpha R) + Q_n^2(\alpha)Q_n^2(\alpha R)] = \cos\alpha(1-R)[Q_n^1(\alpha)Q_n^2(\alpha R) - Q_n^2(\alpha)Q_n^1(\alpha R)], \tag{C2}$$

where two new polynomials are

$$Q_n^1(z) = P_{n-1}^1(z) + P_{n+1}^1(z),$$

$$Q_n^2(z) = P_{n-1}^2(z) + P_{n+1}^2(z). \tag{C3}$$

Using the explicit formulas for $P_\nu^{1,2}(z)$ and expanding the above expressions in square brackets for large α, one gets

$$\sin \alpha\ell[4+O(\alpha^{-2})] = \cos \alpha\ell\left[\frac{1}{\alpha}\frac{2(1-R)(n^2+3/4)}{R}+O(\alpha^{-3})\right].$$

In the lowest order in ℓ, this relation is reduced to $\sin \alpha\ell = 0$, yielding $\alpha_{nk} \simeq \pi k/\ell$. The first-order correction to this result, shown explicitly in Eq. (31), is determined by the above relation. Higher-order corrections can be computed similarly by taking into account higher powers of $1/\alpha$ in Eq. (C3). In practice, there is no need for such an accurate determination of the eigenvalues λ_{nk} with $k>0$. Similarly, one computes the value $v_{nk}(R)$ and the ratio ξ_{nk} given by Eq. (33).

The asymptotic relations (C1) can also be applied to determine α_{nk} and ξ_{nk} for thin spherical layers. For this purpose, one replaces the integer index n by half-integer index $n+1/2$ so that Eq. (C3) becomes

$$q_n^1(z) = P_{n-1/2}^1(z) + P_{n+3/2}^1(z) - P_{n+1/2}^2(z)/z,$$

$$q_n^2(z) = P_{n-1/2}^2(z) + P_{n+3/2}^2(z) + P_{n+1/2}^1(z)/z.$$

In this case, the solutions α_{nk} are determined by Eq. (C2) with $q_n^{1,2}$ instead of $Q_n^{1,2}$. As previously, the expansion in powers of $1/\alpha$ yields Eq. (36). Similar analysis leads to Eq. (37) for ξ_{nk}.

APPENDIX D: RECTANGULAR DOMAIN

As a useful analogy, we consider restricted diffusion in a rectangle with sides π and ℓ, when there is no surface relaxation ($h=0$). The independence of Brownian motion along two coordinates implies factorization of the eigenfunctions:

$$u_{nk}(x,y) = \left(\frac{\epsilon_n}{\sqrt{\pi}}\cos nx\right)\left(\frac{\epsilon_k}{\sqrt{\ell}}\cos \pi k y/\ell\right),$$

with the eigenvalues $\lambda_{nk}=n^2+\pi^2k^2/\ell^2$. If a linear gradient is applied at a given angle θ to the x axis, $B(\mathbf{r})=x\cos\theta + y\sin\theta$, the matrix $\mathcal{B}$ is split in two parts

$$\mathcal{B}_{nk,n'k'} = \delta_{k,k'}\tilde{\mathcal{B}}_{n,n'}\cos\theta + \delta_{n,n'}\tilde{\mathcal{B}}_{k,k'}\sin\theta,$$

where $\tilde{\mathcal{B}}$ is referred to restricted diffusion on the unit interval (its elements can easily be found[1]). As a consequence, the ADC can be written as

$$D(p) = D_x(p)\cos^2\theta + D_y(p)\sin^2\theta,$$

with $D_{x,y}(p)$ corresponding to one-dimensional restricted diffusions along the x and y axes:

$$D_{x,y}(p) = \sum_m \tilde{\lambda}_m \tilde{\mathcal{B}}_{0,m}^2 w(p\tilde{\lambda}_m),$$

where $\tilde{\lambda}_m=\lambda_{m0}=m^2$ for $D_x(p)$ and $\tilde{\lambda}_m=\lambda_{0m}=\pi^2m^2/\ell^2$ for $D_y(p)$. As for thin layers, the orthogonality in two coordinates implies a separation of the ADC in two parts. However, in contrast with thin layers, the separation in length scales does not lead to a region with a constant value in the dependence $D(p)$ on p, showing that separation in lengths is important but insufficient condition for such a tortuosity regime. A rigorous formulation of the sufficient condition for the intermediate (or tortuosity) diffusion regime is still an open problem, especially for porous structures.

[1] D. S. Grebenkov, Rev. Mod. Phys. **79**, 1077 (2007).
[2] P. P. Mitra, P. N. Sen, L. M. Schwartz, and P. Le Doussal, Phys. Rev. Lett. **68**, 3555 (1992).
[3] P. P. Mitra, P. N. Sen, and L. M. Schwartz, Phys. Rev. B **47**, 8565 (1993).
[4] P. N. Sen, Concepts Magn. Reson. **23**, 1 (2004).
[5] B. Robertson, Phys. Rev. **151**, 273 (1966).
[6] R. C. Wayne and R. M. Cotts, Phys. Rev. **151**, 264 (1966).
[7] C. H. Neuman, J. Chem. Phys. **60**, 4508 (1974).
[8] P. T. Callaghan, *Principles of Nuclear Magnetic Resonance Microscopy* (Clarendon, Oxford, 1991).
[9] P. T. Callaghan, A. Coy, D. MacGowan, K. J. Packer, and F. O. Zelaya, Nature (London) **351**, 467 (1991).
[10] P. T. Callaghan, S. L. Codd, and J. D. Seymour, Concepts Magn. Reson. **11**, 181 (1999).
[11] K. R. Brownstein and C. E. Tarr, Phys. Rev. A **19**, 2446 (1979).
[12] A. Caprihan, L. Z. Wang, and E. Fukushima, J. Magn. Reson., Ser. A **118**, 94 (1996).
[13] P. T. Callaghan, J. Magn. Reson. **129**, 74 (1997).
[14] A. V. Barzykin, Phys. Rev. B **58**, 14171 (1998).
[15] A. V. Barzykin, J. Magn. Reson. **139**, 342 (1999).
[16] S. Axelrod and P. N. Sen, J. Chem. Phys. **114**, 6878 (2001).
[17] D. S. Grebenkov, Magn. Reson. Imaging **25**, 559 (2007).
[18] D. S. Grebenkov, Diffus. Fundam. **5**, 1 (2007).
[19] L. J. Zielinski and P. N. Sen, J. Chem. Phys. **119**, 1093 (2003).
[20] D. S. Grebenkov, Phys. Rev. E **76**, 041139 (2007).
[21] H. S. Carslaw and J. C. Jaeger, *Conduction of Heat in Solids*, 2nd ed. (Clarendon, Oxford, 1959).
[22] J. Crank, *The Mathematics of Diffusion*, 2nd ed. (Clarendon, Oxford, 1975).
[23] The vectors U and $\tilde{U}$ depend on the choice of the initial density $\rho(\mathbf{r})$ and the pickup function $\tilde{\rho}(\mathbf{r})$, respectively. When these functions are constant, the integrals (5) and (6) can be found explicitly (see Ref. 39).
[24] The additional factor $2/(2n+1)$ comes from the normalization of the Legendre polynomials.
[25] The ground eigenfunction u_{00} is constant for Neumann boundary condition. The formal substitution of $\alpha_{00}=0$ would require another normalization, so it is more convenient to treat this eigenfunction separately: $u_{00}=\frac{1}{\sqrt{\pi}}\frac{1}{\sqrt{1-R^2}}$.
[26] This definition is obtained by comparing Gaussian-phase approximation (11) and its equivalent form $E\simeq\exp(-b\mathrm{ADC})$, where the b value is conveniently used to represent the combination of control physical parameters. In our dimensionless notations, $b=q^2p<(t_1-t_2)>_2/D$. As pointed out in Ref. 1, this NMR definition (40) is not equivalent to the dynamical definition, when the time-dependent diffusion coefficient appears as a measure of the mean-square displacements in time t (or p): $\mathbb{E}\{[\mathbf{r}(t)-\mathbf{r}(0)]^2\}=2dD(t)t$. In particular, this ADC does not depend on the magnetic field, while $D(p)$ does.
[27] Since the argument of this exponential function contains the difference between integration variables t_1 and t_2, a more careful analysis is required in the vicinity of t_1 close to t_2.
[28] J. W. Haus and K. W. Kehr, Phys. Rep. **150**, 263 (1987).
[29] L. L. Latour, P. P. Mitra, R. L. Kleinberg, and C. H. Sotak, J. Magn. Reson., Ser. A **101**, 342 (1993).
[30] T. M. de Swiet and P. N. Sen, J. Chem. Phys. **104**, 206 (1996).
[31] L. J. Zielinski and P. N. Sen, J. Magn. Reson. **147**, 95 (2000).
[32] D. S. Grebenkov, J. Chem. Phys. **126**, 104706 (2007).
[33] Correction terms in powers of ℓ in Eq. (30) account for curvature effects, i.e., the difference between an interval and a half-circle.
[34] In experiment, the diffusion time T cannot be varied over seven orders of magnitude, as shown in Fig. 2 for the dimensionless parameter p. Among various limiting factors, surface relaxation plays a considerable role, so that a more detailed study of restricted diffusion in thin layers in the presence of surface relaxation would be instructive. Note that the broad range of variation for p can in principle be recovered through the free diffusion coefficient D which takes very different values for liquids and gases.
[35] S. D. Stoller, W. Happer, and F. J. Dyson, Phys. Rev. A **44**, 7459 (1991).
[36] T. M. de Swiet and P. N. Sen, J. Chem. Phys. **100**, 5597 (1994).
[37] M. D. Hürlimann, K. G. Helmer, T. M. de Swiet, P. N. Sen, and C. H.

Sotak, J. Magn. Reson., Ser. A **113**, 260 (1995).
[38] R. Courant and D. Hilbert, *Methods of Mathematical Physics* (Wiley-VCH, New York, 1989), Vol. 1.
[39] Similarly, the integration of Bessel equation (A1) with $\nu=0$ over $[a,b]$ allows for determination of the elements of the vector U (and $\widetilde{U}$) for a uniform initial density $\rho(\mathbf{r})$ (and $\widetilde{\rho}(\mathbf{r})$), involving the integral $\int_a^b drrv = -(rv')_a^b/\alpha^2 = h[bv(b)+av(a)]/\alpha^2$.
[40] Other spatial profiles may also be useful. For instance, a cosine magnetic field in a slab geometry was considered as a model for susceptibility-induced internal fields (Refs. 31 and 32).
[41] We point out on a misprint in Table I (p. 1087) in the review (Ref. 1): the factor $(2n+1)$ is missing in the denominator of both formulas (L11) in the last column (sphere).
[42] I. S. Gradshteyn and I. M. Ryzhik, *Table of Integrals, Series, and Products* (Academic, New York, 1980).